

CrowdVLM-R1: Expanding R1 Ability to Vision Language Model for Crowd Counting using Fuzzy Group Relative Policy Reward

Zhiqiang Wang¹, Pengbin Feng², Yanbin Lin¹,
 Shuzhang Cai³, Zongao Bian⁴, Jinghua Yan⁵, Xingquan Zhu^{1*}
¹Florida Atlantic University ²Amazon.com, Inc. ³University of Texas at Dallas
⁴Georgia Institute of Technology ⁵University of Utah ^{*}Corresponding Author

Abstract—We propose Fuzzy Group Relative Policy Reward (FGRPR), a novel framework that integrates Group Relative Policy Optimization (GRPO) with a fuzzy reward function to enhance learning efficiency. Unlike the conventional binary 0/1 accuracy reward, our fuzzy reward model provides nuanced incentives, encouraging more precise outputs. Experimental results demonstrate that GRPO with a standard 0/1 accuracy reward underperforms compared to supervised fine-tuning (SFT). In contrast, FGRPR, applied to Qwen2.5-VL-(3B/7B), surpasses all baseline models—including GPT-4o, LLaMA2-90B, and SFT—across five in-domain datasets. On an out-of-domain dataset, FGRPR achieves performance comparable to SFT but excels when target values are larger, as its fuzzy reward function assigns higher rewards to closer approximations. This approach is broadly applicable to tasks where the precision of the answer is critical. Code and data: <https://github.com/yeyimilk/CrowdVLM-R1>

Index Terms—Vision language models, large language model, crowd counting, DeepSeek R1, reinforcement learning, group relative policy optimization, fuzzy group relative policy reward, crowd counting.

I. INTRODUCTION

Recently, DeepSeek R1 [1] has drawn much attention among advances in large language models (LLMs), as it demonstrates how reinforcement learning (RL) can be the primary driver of reasoning. The model is a Mixture-of-Experts (MoE) transformer trained using the GRPO algorithm [2]; specifically, it applies simple rule-based rewards to guide the model toward complex reasoning skills.

While DeepSeek R1 is an LLM, its training paradigm can be extended to vision-language models (VLMs). There are various types of visual tasks, such as crowd counting [3]–[5], image classification [6]–[8], and visual question answering [9], [10]; in the context of VLM, they require the model to go beyond simple pattern recognition and perform precise reasoning. Latest works explore applying RL for visual tasks, one of which is VLM-R1 [11], which assigns rewards based on the intersection over union (IoU) score - a binary reward of 1 if $\text{IoU} > 0.5$, and 0 otherwise. However, this approach does not distinguish between near-perfect and marginally correct detections (e.g., an IoU of 0.55 vs. 0.95), then better results do not receive higher rewards. This suggests the need for more

fine-grained reward schemes when applying RL to vision-based reasoning tasks.

In this paper, we develop a novel approach based on GRPO to handle crowd counting tasks. It has been a fundamental yet highly challenging problem and the primary goal is to accurately estimate the number of instances of a particular object. In such scenarios, objects can overlap or vary in size, and they usually fade into complex backgrounds. The VLM must avoid either double-counting or missing partially covered objects. This demands strong spatial reasoning and fine-grained attention.

Therefore, we explore key research questions regarding the application of RL to VLMs for the counting task:

- **RQ1:** How effective is GRPO for VLMs for crowd counting tasks?
- **RQ2:** How can a better reward function be designed to enhance the numerical reasoning ability of VLMs?
- **RQ3:** How to improve VLMs for both within- and cross-domain counting tasks?

To address RQ1, we first conduct a systematic investigation into the impact of RL on VLMs. Specifically, we adapt GRPO, originally used in DeepSeek R1, for fine-tuning mainstream VLMs. Our experiments confirm that GRPO is highly feasible for the counting task in VLMs. However, it requires customized reward function, as conventional reward function has certain limitations.

Issues like this highlights the need to address our RQ2. A well-structured reward function should provide feedback with finer granularity and ensure that slight improvements in counting accuracy are properly incentivized rather than treated as binary outcomes. We solve this research question by introducing a fuzzy group relative policy reward (FGRPR). Our reward function considers both the model’s output format and the numerical precision of its predictions. The format reward is designed as a binary signal to encourage the model to provide an actual count for the scene. Meanwhile, the accuracy reward is based on the difference between the predicted count and the ground truth, guiding the model toward more precise predictions by penalizing deviations from the correct count.

To address RQ3, we create a new, comprehensive counting dataset by selectively combining multiple existing image

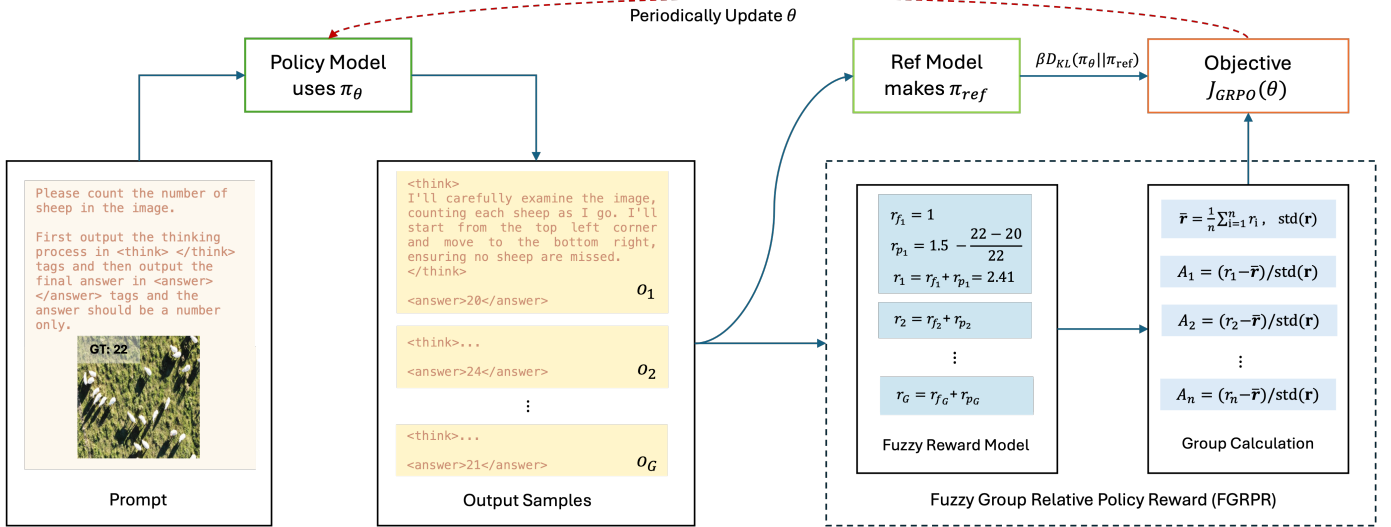


Fig. 1. An overview of our framework which integrates group relative policy optimization (GRPO) and the proposed fuzzy group relative policy reward (FGRPR) to train a visual language model (VLM) for crowd counting tasks. From left to right, an image and prompt are input to a base LLM model to obtain initial counting outcomes (The ground truth value on the top left corner of the input image is just an indicator number for visualization purpose. It is only used for rewards calculation but will not send to LLM as part of input). The instruction model uses a policy model, parameterized by θ , to obtain policy and generate outputs. The proposed fuzzy group relative policy reward is then used to adjust the reward for individual image. The adjusted reward is used to calculate the objective function value, which in term update the θ parameters for supervised fine tuning.

datasets. Given the complexity of the counting task, which involves a wide variety of scenes such as sparse and dense object distributions, as well as large and small objects, we ensure that our dataset captures this diversity. Our goal is to enable the model to adapt to various scene types. Additionally, to evaluate the model’s out-of-domain capabilities, we incorporate the Manatee dataset, which will be used exclusively for testing to assess the model’s zero-shot counting accuracy.

The contributions of this work are as follows:

- We adapt reinforcement learning (GRPO) to train VLMs for crowd counting and propose CrowdVLM-R1, which achieves state-of-the-art performance on the counting task;
- We design a novel fuzzy reward function that takes into account both the format and counting precision, enhancing the model’s ability to provide accurate predictions;
- We introduce a new comprehensive counting dataset, offering diverse scenes to assess the model’s counting capabilities for in-domain and out-of-domain scenes.

II. RELATED WORK

Traditional methods for Crowd Counting. Early research on Crowd Counting can be grouped into three categories: detection-based, regression-based and density estimation-based methods. Detection-based approaches typically utilize detectors for a specific object, e.g., human head or animal body, and perform counting based on the detection results [12]–[14]. These methods have achieved good accuracy for sparse scenes, but struggle under dense or occluded scenarios. Regression-based methods, on the other hand, maps the image patches directly to the count of objects via regression techniques [15]–[17]. Density estimation methods get rid of

learning to localize individual objects by estimating the count with density maps [18]–[20].

With the success of Convolution Neural Networks (CNNs) in multiple computer vision tasks, researchers start to leverage CNNs to learning non-linear mappings from crowd images to counts. CNNs have been proven to extract features of higher quality than traditional methods for many vision tasks including counting [21]. Among numerous CNN-based approaches, early works such as [22], [23] use CNN models to perform end-to-end regression without significant modification of the model architecture. Subsequent research has focused on enhancing model architectures [24]–[29]. Examples include multi-stage CNNs [28], which are designed to adapt to counting scenes with different scales and distortion, and Mixture of CNNs [29] with a mixture-of-expert approach where each CNNs is specialized to a different scene.

Vision-Language Models (VLMs) for Counting. The need for supervision and labeling of datasets limits the generalizability of both CNN-based and non-CNN-based methods. Recent vision-language pretraining [30] [31] stop relying on supervised training by learning from an extremely large number of image-text pairs. VLMs generates high quality visual-textual features, which are adaptable to a broad spectrum of open-world downstream tasks. Recent VLM-based counting methods have demonstrated superior performance compared to class-specific approaches in counting accuracy [32]–[37]. These approaches establish a joint embedding space that connects images with textual inputs, hence enable models to comprehend general concepts learned during extensive pretraining.

Reasoning enhancement for Large Language Models. As LLM’s capabilities advance, there is a growing research focus

on their reasoning abilities. A recent work, DeepSeek R1 [1], utilizes pure reinforcement learning with rule-based reward and demonstrates strong performance on a series of reasoning tasks. This approach can be naturally extended to the multi-modality setting and applied to VLMs [38]–[41].

III. METHOD

In this section we present our approach to improving VLM-based counting through reinforcement learning. We begin by introducing Group Relative Policy Optimization (GRPO) and highlighting its advantages over previous RL methods. Next, we propose a novel fuzzy group relative policy reward (FGRPR), which refines the reward structure by accounting for both output format adherence and numerical precision. Finally, we outline our overall framework, which integrates GRPO and FGRPR into the training pipeline of our proposed model, CrowdVLM-R1, to improve its counting performance across diverse datasets and real-world scenarios.

A. Group Relative Policy Optimization

The GRPO [2] is an RL algorithm derived as a variant of Proximal Policy Optimization (PPO) [42]. This algorithm was introduced by the Deepseek group, extending the PPO framework to incorporate group-based optimization strategies. The value function used in PPO is typically implemented as a separate model of comparable size to the policy model, introducing significant memory and computational overhead. By utilizing the average reward of multiple sampled outputs generated in response to the same input as the baseline, GRPO eliminates the need for an additional value function approximation. This approach reduces both computational complexity and memory overhead, while maintaining effective variance reduction in policy gradient updates.

For standardized GRPO, given an input question q , a group of G outputs $\mathbf{o} = \{o_1, o_2, \dots, o_G\}$ are generated from a sampling process determined by the old policy $\pi_{\theta_{\text{old}}}$, parameterized by θ , to answer the question q . Let $\mathbf{r} = \{r_1, r_2, \dots, r_G\}$ denotes G rewards in the group and $\bar{\mathbf{r}}$ is the group average reward, the advantages $\hat{A}_{i,t}$ of all tokens in the output as the normalized reward will be

$$\hat{A}_{i,t} = \tilde{r}_i = \frac{r_i - \bar{\mathbf{r}}}{\text{std}(\mathbf{r})} \quad (1)$$

The policy model will be optimized by maximizing the objective:

$$\begin{aligned} \mathcal{J}_{GRPO}(\theta) = & \mathbb{E}_{q \sim P(Q), \{o_i\}_{i=1}^G \sim \pi_{\theta_{\text{old}}}(O|q)} \\ & \frac{1}{G} \sum_{i=1}^G \frac{1}{|o_i|} \sum_{t=1}^{|o_i|} \left\{ \min \left[\frac{\pi_{\theta}(o_{i,t}|q, o_{i,<t})}{\pi_{\theta_{\text{old}}}(o_{i,t}|q, o_{i,<t})} \hat{A}_{i,t}, \right. \right. \\ & \left. \left. \text{clip} \left(\frac{\pi_{\theta}(o_{i,t}|q, o_{i,<t})}{\pi_{\theta_{\text{old}}}(o_{i,t}|q, o_{i,<t})}, 1 - \epsilon, 1 + \epsilon \right) \hat{A}_{i,t} \right] \right. \\ & \left. - \beta D_{KL}[\pi_{\theta} || \pi_{\text{ref}}] \right\} \end{aligned} \quad (2)$$

where ϵ and β are hyperparameters, and $\hat{A}_{i,t}$ represent the advantage computed based on the relative rewards of outputs within each group. π_{θ} is the current policy to be optimized,

generated by the trainable policy model, typically an LLM or sequence model, parameterized by θ . π_{old} is the behavior policy used for sampling, which comes from a frozen model of the policy π_{θ} from a previous iteration. π_{ref} is the reference policy for KL penalty, which is typically from the SFT model (also a LLM or sequence model), trained with human data.

GRPO determines which strategies should be retained or improved by comparing the performance of a group of samples, rather than relying on the absolute reward of a single sample. This approach is analogous to the process of natural selection, where only strategies that outperform the average are allowed to survive and evolve further. This group-based method makes GRPO more stable when handling diverse tasks, as it no longer depends on the performance of a single sample but instead leverages the collective intelligence of the group to evaluate the quality of strategies.

PPO employs a clipped objective function to limit the magnitude of policy updates. However, this clipping mechanism can sometimes overly restrict updates, leading to slower convergence. On the other hand, TRPO ensures the stability of policy updates through a strict KL divergence constraint, but its optimization process requires second-order methods (e.g., conjugate gradient), resulting in high computational costs that make it unsuitable for large-scale reinforcement learning tasks. GRPO addresses these limitations by combining clipping mechanisms with a KL divergence term, ensuring a balance between exploration and stability. This balance makes GRPO more reliable in complex tasks, as it maintains both stability and consistency during optimization. While PPO's fixed clipping range may limit the convergence speed of policies, GRPO introduces a dynamic adjustment mechanism (e.g., through a beta parameter) to adaptively control the policy update range, effectively adjusting the KL divergence to achieve stable and efficient policy updates.

In previous work like VLM-R1 [11], a typical GPRO accuracy reward is defined as

$$r_a = \begin{cases} 1, & \frac{|\hat{y} - y|}{y} < 0.5 \\ 0, & \text{otherwise} \end{cases} \quad (3)$$

where \hat{y} is the count predicted by the model and y denotes the real count. This is a "fixed reward" that assigns 1 to any prediction values lie in the range $(\frac{y}{2}, \frac{3y}{2})$. For example, if the image contains 500 persons, the prediction values of 260, 500, 740 share the same reward and have no difference from model perspective. However, these values are supposed to have different rewards for their different accuracies.

B. FGRPR: Fuzzy Group Relative Policy Reward

To enable SFT by using multiple sources of crowd counting data, we introduce FGRPR method, which employs a fuzzy reward function to gauge the fine-tuning of the R1 model by taking quality of counting, compared to the benchmark, for consideration.

Overall, the reward function consists of two parts: *format reward*, r_f , and *precision reward*, r_p which are linearly combined in Eq. (4).

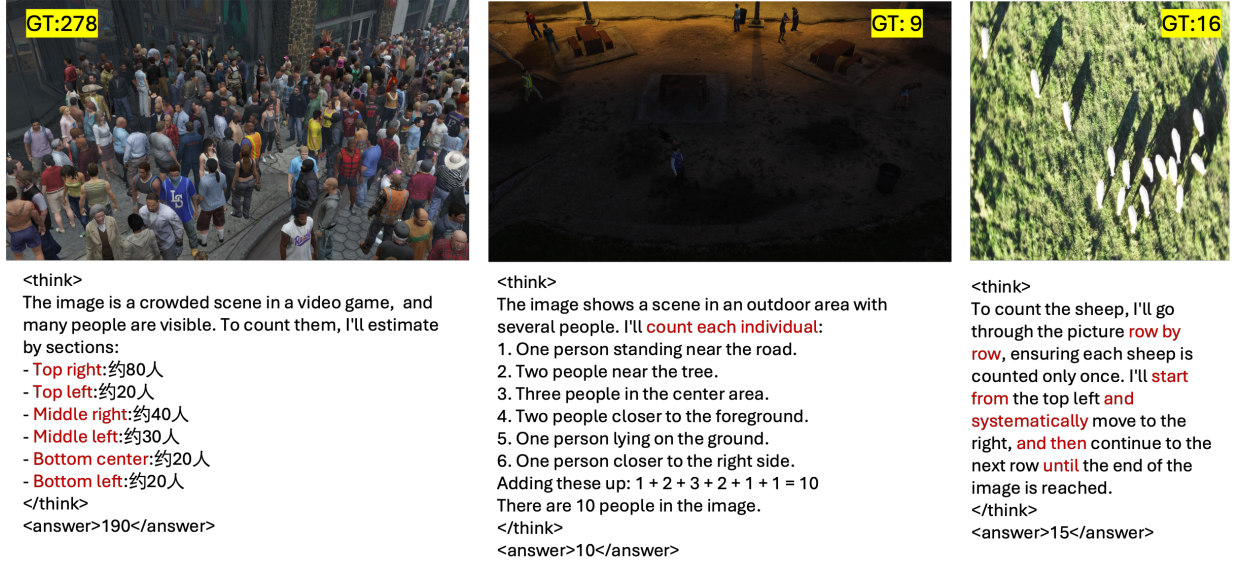


Fig. 2. Examples of model outputs at during the training stage, showing various counting strategies. In the left image, where the crowd is dense and difficult to count, the model segments the scene into six regions and estimates the number of individuals in each. In the middle image, with only a few people, the model counts them individually. In the right image, which has a moderate density of sheep, the model scans row by row to ensure each entity is counted once. These strategies resemble human approaches to counting in different scenarios.

$$r = r_f + r_p \quad (4)$$

$$r(s, a) = \mu_f(s, a) \cdot r_f(s, a) + \mu_p(s, a) \cdot r_p(s, a) \quad (5)$$

The format reward is straightforward, that is, if the model output $\text{format}(\hat{y}_p)$, follows the defined $\text{format}(\mathbb{F})$, r_f is 1, otherwise, r_f is 0.

$$r_f = \begin{cases} 1, & \text{if } \hat{y}_p = \mathbb{F} \\ 0, & \text{otherwise} \end{cases} \quad (6)$$

Previous work and research topics indicated that the answers can be or simply categorized as “Yes” or “No” which means the precision reward can be easily used with binary value, “1” or “0”. While the crowd counting task also has a “ground true” value, we prefer to have a fuzzy reward to represent the model estimated value that it should have a higher reward when the answer is closer to number of objects and lower reward or even 0 if the predicted value is far away from the “ground truth” value. Thus, the precision reward in our task is defined as shown below.

$$r_p = \begin{cases} 1.5 - \frac{|\hat{y} - y|}{y}, & \frac{|\hat{y} - y|}{y} < 0.5 \\ 0, & \text{otherwise} \end{cases} \quad (7)$$

where \hat{y} is the count predicted by the model and y denotes the real count. The reward values fall within the range $0 \cup (1, 1.5]$. The reason of the range $(1, 1.5]$ instead of $(0.5, 1]$ is motivated by the nature of the counting task, where prediction accuracy is prioritized over formatting. As a result, higher rewards are assigned when the model produces near-correct predictions, emphasizing the importance of accuracy.

C. Framework

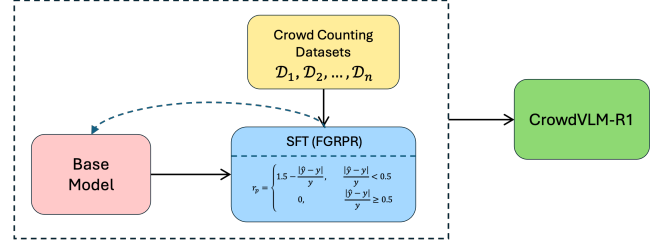


Fig. 3. A conceptual view of R1 model expansion to vision language model for crowd counting (CrowdVLM+R1) using fuzzy group relative policy reward. Multiple crowd-sourced inputs, with ground-truth counting numbers, are used for supervised fine tuning. The inputs are fed into to a base model to generate outcomes, followed by the proposed fuzzy group relative policy reward (FGRPR) to determine individual rewards and system objective function value $\mathcal{J}_{GRPO}(\theta)$. Gradient propagation process is then applied to update θ , and in terms improve the base model for better counting results.

Fig. 3 presents the general idea of training a CrowdVLM-R1 model. Instead of using a labeled dataset to fine-tune the based instruct model to optimize its performance directly, in our method, GRPO is employed during the SFT stage with verifiable rewards (Equ. 4, including format reward (Equ. 6) and counting precision reward (Equ. 7).

For details, our proposed framework is shown in Fig. 1. A structured prompt comprises a natural language description (including the counting task and the expected output format) and an input image. This prompt is input into a policy model—implemented as a LLM—which defines the learner policy π_θ and autoregressively generates a set of candidate outputs $\{o_1, o_2, \dots, o_G\}$. Each output o_i consists of a step-by-step reasoning process and a predicted count corresponding to

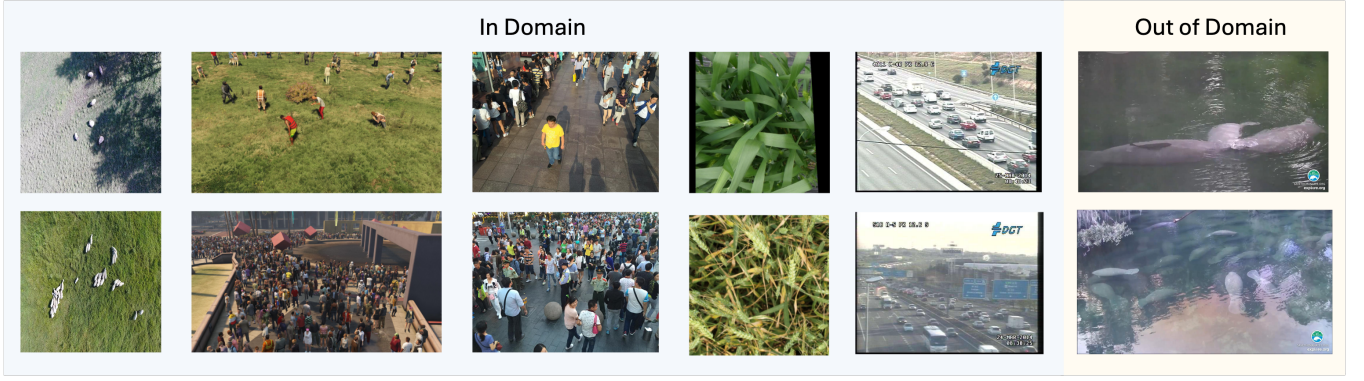


Fig. 4. This figure presents the image examples from test dataset where each column comes from the same original dataset and the first row shows an easier counting task while the second one is more complex within their original data sources.

TABLE I
DATASET SUMMARY

Dataset	Type	Sheep	Video Game Characters	Street Pedestrians	Wheat Heads	Cars	Manatees*
Training	Samples	1000	1000	400	1000	403	-
	Min count	1	5	12	1	9	-
	Max count	105	3546	578	125	95	-
	Mean count	31	326	123	45	34	-
Testing	Samples	100	100	100	100	100	100
	Min count	1	13	9	1	15	1
	Max count	103	1709	514	115	107	50
	Mean count	29	365	514	49	42	16

* Out-of-domain dataset.

the target objects in the input image. Subsequently, a reward model evaluates these generated responses, which assigns a scalar reward r_i to each output. The reward r_i is composed of two components: a format reward r_{f_i} and a prediction reward r_{p_i} , as detailed in Section III-B. These individual rewards are then aggregated to compute group-wise advantages A_i for all G outputs, reflecting the relative quality of each sampled response. Our objective function $\mathcal{J}_{\text{GRPO}}(\theta)$ is formulated using the computed advantages A_i (for $i = 1, \dots, G$) and a KL-divergence regularization term $D_{\text{KL}}(\pi_{\theta} \parallel \pi_{\text{ref}})$, scaled by a hyperparameter β in Equation (2). Here, in our case, the reference model is an SFT LLM model trained with human data. We will minimize the objective/loss function using gradient ascent (or descent on the negative objective). After the calculation, the gradient signal will flow from the objective back into the policy model to update its parameters θ based on both the relative advantages and the regularization signal. After sufficient interactions, we will finally receive a trained-well LLM model that can count the number of specified targets in a given image.

IV. EXPERIMENT

A. Dataset

The dataset used in this article is derived from existing datasets for counting tasks. The training dataset includes

aerial sheep [43], video game characters from GTAV_Head [44], street pedestrians [27], wheat heads from the Global Wheat Head Detection (GWHD) dataset [45] and cars from TRANCOS [46]. The testing dataset includes an additional dataset, manatee [47], for out-of-domain evaluation.

Fig. 4 shows two examples from each original dataset. The images in the first row are clearer, with lower-density objects, making the counting task easier, while the images in the second row depict more complex scenarios with a higher density of objects, increasing task difficulty.

Within our dataset, not all the images from original datasets were used. If original dataset has train and test sets, then the original train and test samples were picked randomly to use as part of our own train and test set, respectively. If the original data set was not split into train and test set, then the dataset was split into two parts first and then images from these two subsets were picked later into our train and test sets. For our dataset dataset, up to 1000 images and 100 samples were choose for each of the original datasets.

Table I provides a summary of the datasets used in our study, highlighting the diversity and complexity of the counting task. The dataset encompasses a wide range of scenarios, from relatively simple images containing only a few objects to highly complex scenes with thousands of densely packed, overlapping instances. The variation in object counts, as indicated by

TABLE II
PERFORMANCE COMPARISON OF MODELS ACROSS DOMAINS.

Model	In-Domain										Out-Domain		Overall	
	Sheep		Characters		Pedestrians		Wheat Heads		Cars		Manatees			
	MAE	RMSE	MAE	RMSE	MAE	RMSE	MAE	RMSE	MAE	RMSE	MAE	RMSE	MAE	RMSE
Sonnet-3.5	8.79	13.48	191.10	298.53	55.96	86.77	36.99	44.04	14.40	17.99	9.44	15.12	52.78	128.66
In-VL2-26B	14.13	22.75	271.96	422.56	64.19	101.23	33.64	41.24	22.40	31.74	8.22	12.99	69.09	178.98
GPT-4o	7.12	11.73	243.41	504.93	58.36	85.27	39.79	46.58	17.22	23.56	5.82	10.20	61.95	210.24
LLaMA-90B	3.87	7.54	182.40	298.53	28.60	38.02	18.18	21.91	19.24	27.31	5.70	10.54	44.68	127.73
Q-3B	14.11	21.60	277.67	450.83	76.04	122.38	40.34	47.07	22.83	29.71	11.03	16.98	73.67	192.39
Q-7B	12.03	20.42	347.44	536.23	121.99	166.07	47.82	55.31	40.24	44.24	11.49	17.26	96.83	231.25
Q-3B-SFT	4.19	6.93	104.34	199.79	33.38	52.43	18.57	23.67	10.68	13.25	8.15	13.40	29.89	85.27
Q-7B-SFT	4.86	8.24	97.41	224.39	24.78	42.39	18.51	25.22	11.63	14.55	7.93	13.21	27.52	94.20
Q-3B-R1	5.75	9.15	97.43	184.97	41.74	62.71	25.99	30.34	14.78	17.73	8.92	14.39	32.44	81.32
Q-7B-R1	8.04	13.20	145.55	261.81	32.29	56.10	22.68	27.40	14.42	18.25	9.88	15.26	38.81	110.44
Q-3B-FR	4.19	8.07	85.52	171.28	24.02	38.76	18.86	23.11	10.55	14.00	7.81	13.25	25.16	72.81
Q-7B-FR	3.33	6.24	88.10	170.17	20.60	40.89	14.52	18.74	9.71	12.47	8.16	13.23	24.07	72.28

Q: Qwen-VL-2.5-Instruct; R1: model was trained with GRPO; FR: model was trained with FGRPR;

the minimum, maximum, and mean values, demonstrates the challenge of accurately estimating quantities across different contexts. Some datasets, such as the video game characters and street pedestrians, include images where objects are densely clustered, making separation and identification difficult. Additionally, environmental noise, including buildings, trees, and other background elements, further complicates detection in real-world scenes. The dataset complexity indicates the challenges of doing counting task for a single model.

B. Experiment Setup

1) Models:

- **Baseline Models:** We evaluate several widely used benchmark models, including GPT-4o-2024-11-20 (*GPT-4o*), Claude Sonnet-3.5-2024-06-20 (*Sonnet-3.5*), LLaMA 2-90B (*LLaMA-90B*), Intern-VL-26B (*In-VL2-26B*), Qwen2.5-VL-3B (*Q-3B*), and Qwen2.5-VL-7B (*Q-7B*).
- **SFT Models:** For comparative purposes, we perform supervised fine-tuning on Qwen2.5-VL-3B (*Q-3B-SFT*) and Qwen2.5-VL-7B (*Q-7B-SFT*).
- **GRPO Models:** We conduct full-scale reinforcement learning (RL) training with the GRPO method on Qwen2.5-VL-3B (*Q-3B-R1*) and Qwen2.5-VL-7B (*Q-7B-R1*), employing the standard accuracy-based reward defined in Equ. 3.
- **CrowdVLM-R1 Models (Ours):** We also perform full-scale RL training using our proposed FGRPR method on Qwen2.5-VL-3B (*Q-3B-FR*) and Qwen2.5-VL-7B (*Q-7B-FR*). Our fuzzy reward function, defined in Equ. 4.

2) *Experimental Environment:* During training and testing for GRPO and FRGPR, we use 8 Nvidia L40S GPU (each

46GB memory). The training dataset consists of 3803 images and 5 classes, the experiment is set have max prompt length 1024, number of generations 8, per device training batch size 6, gradient accumulation steps 2, data types bf16, and epochs 2. The testing consists of 600 images and 6 classes (one class is out of training samples), we uses batch size 2 and data types bf16. It is worth noting that we use the same training and testing hyperparameters and prompt method across all the reinforcement learning models.

C. Evaluation Metrics

To evaluate the performance of crowd counting task, we employ Mean Absolute Error (MAE) and Root Mean Squared Error (RMSE), which are standard metrics in the field. MAE measures the average absolute difference between predicted and actual crowd counts, providing an intuitive measure of accuracy:

$$\text{MAE} = \frac{1}{n} \sum_{i=1}^n |y_i - \hat{y}_i| \quad (8)$$

where y_i and \hat{y}_i represent the ground truth and predicted counts, respectively, and n is the total number of samples.

RMSE, defined as the square root of the mean squared differences, penalizes larger errors more heavily, making it particularly useful when significant deviations are critical for evaluation:

$$\text{RMSE} = \sqrt{\frac{1}{n} \sum_{i=1}^n (y_i - \hat{y}_i)^2} \quad (9)$$

While both metrics indicate model accuracy, MAE provides a straightforward interpretation of average error, whereas

TABLE III
PERFORMANCE COMPARISON OF MODELS ACROSS RANGES.

Model	In-Domain						Out-Domain			
	[1-20]		[21-50]		[51, -]		[1-20]		[21-50]	
	MAE	RMSE	MAE	RMSE	MAE	RMSE	MAE	RMSE	MAE	RMSE
Q-3B-SFT	2.99	5.40	8.37	10.69	64.13	134.20	1.83	3.25	17.62	20.81
Q-7B-SFT	2.65	4.47	7.39	9.08	59.15	148.47	1.50	2.66	17.57	20.63
Q-3B-R1	3.21	4.93	11.49	13.75	67.82	127.66	1.70	3.08	19.75	22.43
Q-7B-R1	3.43	5.96	11.87	14.57	83.00	173.86	2.15	3.56	21.48	23.74
Q-3B-FR	3.06	5.00	8.26	10.42	52.51	114.42	1.60	2.91	17.12	20.64
Q-7B-FR	2.43	4.60	6.95	9.38	50.83	113.66	1.80	3.26	17.70	20.53

Q: Qwen-VL-2.5-Instruct; R1: model was trained with GRPO; FR: model was trained with FGRPR

RMSE emphasizes larger errors by amplifying their impact. Lower values for both metrics signify better performance.

In order to have a comprehensive analysis, we also employ R^2 , MAPE, Pearson’s correlation, and Spearman’s correlation. Their formal definitions can be found in Section VI-A.

D. Results

The overall model performance across different domains is shown in Table II. Among the baseline models, *LLaMA-90B* demonstrates outstanding performance in four of the six domain datasets. Nevertheless, *GPT-4o* and *Sonnet-3.5* achieve lower MAE and RMSE scores compared to *LLaMA-90B*. Specifically, *GPT-4o* exhibits comparable performance to *LLaMA-90B* on the out-of-domain dataset (*manatee*), displaying an MAE of approximately 5.7 and an RMSE around 10. On the other hand, *Q-3B* and *Q-7B* consistently show among the poorest metric results across all six datasets.

However, after traditional supervised fine-tuning (SFT), both *Q-3B-SFT* and *Q-7B-SFT* improve significantly. Specifically, they outperform not only their base versions but also all baseline models, including state-of-the-art models such as *GPT-4o* and *LLaMA-90B*, across five in-domain datasets. Although *Q-7B-SFT* achieves a lower overall MAE compared to *Q-3B-SFT*, its performance is not consistently better across these five in-domain datasets. Furthermore, *Q-7B-SFT* presents a higher RMSE value, indicating that its prediction errors exhibit greater variance and instability.

After fine-tuning with GRPO methods employing the traditional 0/1 reward function (rewarding predictions with 1 if $\frac{\hat{y}-y}{y} < 0.5$, otherwise 0), the results indicate that although this approach has some effectiveness, the models *Q-3B-R1* and *Q-7B-R1* show worse performance than their corresponding directly fine-tuned counterparts, *Q-3B-SFT* and *Q-7B-SFT*. This outcome reveals a limitation of applying such a GRPO-based reward approach specifically for the crowd counting task.

Models trained with our proposed FGRPR method, particularly *Q-7B-FR*, exhibit state-of-the-art performance across

all five in-domain datasets. They continue to reduce the MAE and RMSE compared to the previously best-trained model, *Q-7B-SFT*, showing consistency in error reduction. For the 3B variant, *Q-3B-FR* achieves better performance than the previous SFT model (*Q-3B-SFT*) in two datasets, slightly worse performance in sheep counting, and equivalent performance in wheat head and traffic car counting datasets. Moreover, for the out-of-domain dataset, SFT and FGRPR shows similar performance that they improved compared to their based models that shows better performance than bigger models *In-VL2-26B* and *Sonnet-3.5* but still can not achieve to the best industry models like *GPT-4o* and *LLaMA-90B*. Considering the small size of our base models(only 3B and 7B), these results collectively prove the effectiveness of our proposed FGRPR reward function.

This can be further confirmed by Table III that models are evaluated by the ranges. In domain datasets, while SFT and FGRPR methods have similar in relatively few objects counting, range [1-20] and [21-50], when object continue growing over 50, FGRPR shows dominant performance over SFT and GRPO which controlled by accuracy reward, Equ.3, of r_a . This shows the effectiveness of our reward function, Equ.7, the part of $\frac{|\hat{y}-y|}{y}$ which provides higher reward with better counting value.

This effectiveness is further supported by Table III, where the models are evaluated based on different count ranges. In in-domain datasets, the SFT and FGRPR methods have similar performance with fewer objects, in ranges [1-20] and [21-50]. However, as object counts exceed 50, FGRPR shows superior performance compared to SFT and GRPO, which is guided by the accuracy reward, Equ. ?? . This highlights the effectiveness of our proposed reward function, Equ. ?? , particularly the component $(\frac{|\hat{y}-y|}{y})$, which offers higher rewards for more accurate counts.

E. Analysis

1) *Model rewards*: In Fig. 5, all four models demonstrate an upward trend in both precision and format rewards, as shown in the first-row subfigures where a simple moving

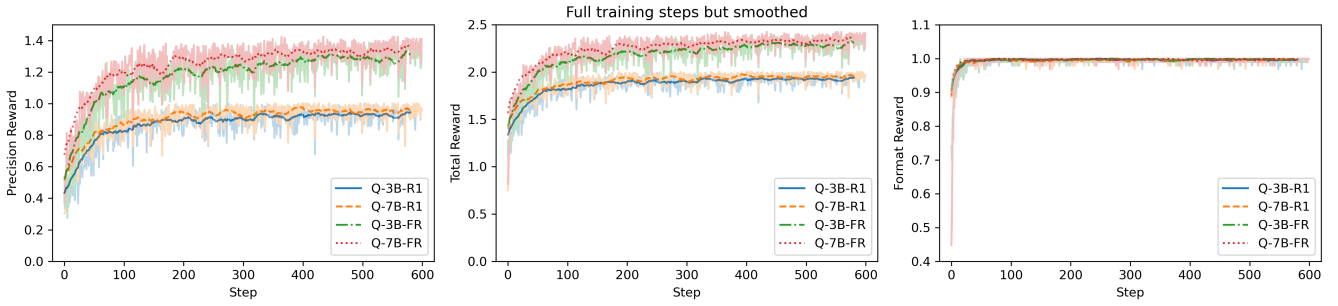


Fig. 5. Training reward curves for different models show the same trend while for precision reward, bigger models dominate the smaller models within the same method over the training steps after smoothed. And their format reward lines do not have any difference after 100 steps.

TABLE IV
ADDITIONAL PREDICTION MEASUREMENTS

Metrics	R^2	MAPE	Pearson	Spearman
Value	0.8795	0.2389	0.9655	0.9497

average with a window size of 20 is applied across 600 training steps. The 7B models start at higher points than the 3B models, indicating superior initial performance, consistent with prior studies that larger models typically outperform smaller ones within the same family. While 3B with FGRPR has similar start values with *Q-7B-R1*.

All four models display a sharp increase within the initial 100 training steps, followed by fluctuating yet steady improvement in precision rewards over the subsequent 500 steps, reaching their peak around step 600. Notably, the FGRPR method demonstrates a sharper and steadier growth trajectory compared to the traditional GRPO method. Furthermore, the continuous upward trend shown by the FGRPR model at the training endpoint suggests potential for further improvement with additional training data or a longer training period, whereas models trained via GRPO with traditional rewards plateau and exhibit little to no increase in reward values during the second half of training. Meanwhile, all four models have identical format reward curves, as they share the same format reward function.

Despite the clear overall trends revealed by smoothing, the shadows in Fig. 5 illustrate considerable fluctuations in reward values throughout training. At certain training steps, precision reward values drop abruptly before subsequently recovering and reconnecting with the general upward trend.

2) *Concentrated results*: Fig. 6 presents distribution statistics for ground truth over prediction results. The histogram and density plots show both distributions are highly right-skewed, with the majority of values concentrated below 250. However, the second row subfigures dramatically illustrate disparity between GT and predictions - GT values show numerous outliers spanning a much wider range, while predicted values display fewer outliers and compressed variability.

Table IV reveals additional metrics for the prediction of the model. The R^2 value of 0.8795 indicates that the model

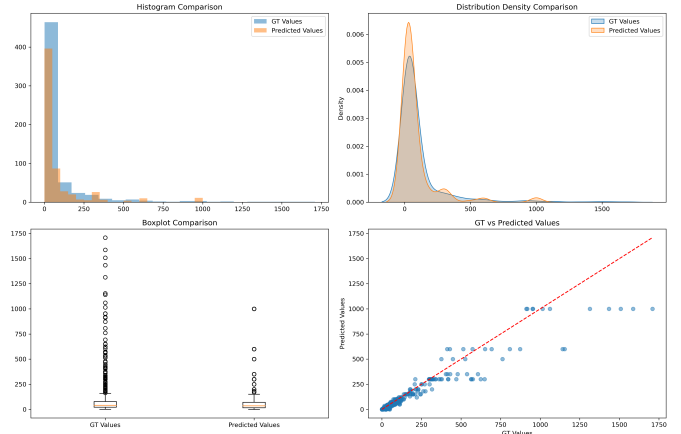


Fig. 6. Distribution statistics comparison between true values and predicted values. Results from model *Q-7B-RF*.

explains nearly 88% of the variance. Strong correlation coefficients (Pearson = 0.9655, Spearman = 0.9497) confirming the model generally preserves rank ordering. And A MAPE of 23.89% suggests predictions are, on average, off by about a quarter of the true value.

In conclusion, while the model shows a good performance in some ways, especially when below 250 counts, there are limitations. It produced concentrated predictions that don't reflect the true distribution's variability and it was also focused heavily on certain values.

V. CONCLUSION

The success of DeepSeek R1 highlights the effectiveness of RL in enhancing the reasoning abilities of LLMs for complex tasks, such as solving math problems. This approach has been extended to VLMs for tasks like interpreting mathematical figures. Previous work often used a simplistic "0/1" reward model, reducing answers to binary outcomes like "YES/NO". However, this reward function is inadequate for problems that don't require exact matches, such as crowd counting or position matching with intersection over union (IOU).

To address this, we proposed FGRPR, which leverages the robust RL method, GRPO, combined with a fuzzy reward system that assigns higher rewards for values closer to the

ground truth. Our experiments demonstrate that the traditional “0/1” reward model with GRPO underperforms compared to SFT in these tasks. In contrast, FGRPR shows superior performance across all models, even surpassing *GPT-4o* and *LLaMA-90B* in in-domain datasets.

While FGRPR performs comparably to SFT in out-of-domain datasets with smaller target values, it excels with larger targets. This makes sense since traditional RL methods disregard the distinction between $\frac{y}{2}$ and $\frac{3y}{2}$. When y is smaller, although our method remains competitive, it doesn’t always provide an advantage where can be improved in the future.

Although this research specifically evaluates the effectiveness of FGRPR within the domain of crowd counting, the framework we propose can easily be generalized and applied to other estimation tasks where fuzzy reward evaluations are beneficial.

REFERENCES

- [1] D. Guo, D. Yang, H. Zhang, J. Song, R. Zhang, R. Xu, Q. Zhu, S. Ma, P. Wang, X. Bi *et al.*, “Deepseek-r1: Incentivizing reasoning capability in llms via reinforcement learning,” *arXiv preprint arXiv:2501.12948*, 2025.
- [2] Z. Shao, P. Wang, Q. Zhu, R. Xu, J. Song, X. Bi, H. Zhang, M. Zhang, Y. Li, Y. Wu *et al.*, “Deepseekmath: Pushing the limits of mathematical reasoning in open language models,” *arXiv preprint arXiv:2402.03300*, 2024.
- [3] C. Zhang, H. Li, X. Wang, and X. Yang, “Cross-scene crowd counting via deep convolutional neural networks,” in *Proceedings of the IEEE conference on computer vision and pattern recognition*, 2015, pp. 833–841.
- [4] W. Liu, M. Salzmann, and P. Fua, “Context-aware crowd counting,” in *Proceedings of the IEEE/CVF conference on computer vision and pattern recognition*, 2019, pp. 5099–5108.
- [5] D. Liang, J. Xie, Z. Zou, X. Ye, W. Xu, and X. Bai, “Crowdclip: Unsupervised crowd counting via vision-language model,” in *Proceedings of the IEEE/CVF conference on computer vision and pattern recognition*, 2023, pp. 2893–2903.
- [6] Q. Li, W. Cai, X. Wang, Y. Zhou, D. D. Feng, and M. Chen, “Medical image classification with convolutional neural network,” in *2014 13th international conference on control automation robotics & vision (ICARCV)*. IEEE, 2014, pp. 844–848.
- [7] S. Menon and C. Vondrick, “Visual classification via description from large language models,” *arXiv preprint arXiv:2210.07183*, 2022.
- [8] Y. Qi, S. Cai, Z. Zhao, J. Li, Y. Lin, and Z. Wang, “Benchmarking large language models for image classification of marine mammals,” *arXiv preprint arXiv:2410.19848*, 2024.
- [9] S. Antol, A. Agrawal, J. Lu, M. Mitchell, D. Batra, C. L. Zitnick, and D. Parikh, “Vqa: Visual question answering,” in *Proceedings of the IEEE international conference on computer vision*, 2015, pp. 2425–2433.
- [10] J. Guo, J. Li, D. Li, A. M. H. Tiong, B. Li, D. Tao, and S. Hoi, “From images to textual prompts: Zero-shot visual question answering with frozen large language models,” in *Proceedings of the IEEE/CVF conference on computer vision and pattern recognition*, 2023, pp. 10 867–10 877.
- [11] H. Shen, Z. Zhang, K. Zhao, Q. Zhang, R. Xu, and T. Zhao, “Vlm-r1: A stable and generalizable r1-style large vision-language model,” <https://github.com/om-ai-lab/VLM-R1>, 2025, accessed: 2025-02-15.
- [12] J. Lin and L. S. Davis, “Shape-based human detection and segmentation via hierarchical part-template matching,” *IEEE transactions on pattern analysis and machine intelligence*, vol. 32, no. 4, pp. 604–618, 2010.
- [13] M. Wang and X. Wang, “Automatic adaptation of a generic pedestrian detector to a specific traffic scene,” in *CVPR 2011*. IEEE, 2011, pp. 3401–3408.
- [14] B. Wu and R. Nevatia, “Detection of multiple, partially occluded humans in a single image by bayesian combination of edgelet part detectors,” in *Tenth IEEE International Conference on Computer Vision (ICCV’05) Volume 1*, vol. 1. IEEE, 2005, pp. 90–97.
- [15] A. B. Chan, Z.-S. J. Liang, and N. Vasconcelos, “Privacy preserving crowd monitoring: Counting people without people models or tracking,” in *2008 IEEE conference on computer vision and pattern recognition*. IEEE, 2008, pp. 1–7.
- [16] K. Chen, S. Gong, T. Xiang, and C. Change Loy, “Cumulative attribute space for age and crowd density estimation,” in *Proceedings of the IEEE conference on computer vision and pattern recognition*, 2013, pp. 2467–2474.
- [17] K. Chen, C. C. Loy, S. Gong, and T. Xiang, “Feature mining for localised crowd counting,” in *Bmvc*, vol. 1, no. 2, 2012, p. 3.
- [18] Z. Wang, H. Liu, Y. Qian, and T. Xu, “Crowd density estimation based on local binary pattern co-occurrence matrix,” in *2012 IEEE International Conference on Multimedia and Expo Workshops*. IEEE, 2012, pp. 372–377.
- [19] V. Lempitsky and A. Zisserman, “Learning to count objects in images,” *Advances in neural information processing systems*, vol. 23, 2010.
- [20] L. Fiaschi, U. Köthe, R. Nair, and F. A. Hamprecht, “Learning to count with regression forest and structured labels,” in *Proceedings of the 21st international conference on pattern recognition (ICPR2012)*. IEEE, 2012, pp. 2685–2688.
- [21] P. Sermanet, D. Eigen, X. Zhang, M. Mathieu, R. Fergus, and Y. LeCun, “Overfeat: Integrated recognition, localization and detection using convolutional networks,” *arXiv preprint arXiv:1312.6229*, 2013.
- [22] C. Wang, H. Zhang, L. Yang, S. Liu, and X. Cao, “Deep people counting in extremely dense crowds,” in *Proceedings of the 23rd ACM international conference on Multimedia*, 2015, pp. 1299–1302.
- [23] M. Fu, P. Xu, X. Li, Q. Liu, M. Ye, and C. Zhu, “Fast crowd density estimation with convolutional neural networks,” *Engineering Applications of Artificial Intelligence*, vol. 43, pp. 81–88, 2015.
- [24] D. Babu Sam, S. Surya, and R. Venkatesh Babu, “Switching convolutional neural network for crowd counting,” in *Proceedings of the IEEE conference on computer vision and pattern recognition*, 2017, pp. 5744–5752.
- [25] D. Onoro-Rubio and R. J. López-Sastre, “Towards perspective-free object counting with deep learning,” in *European conference on computer vision*. Springer, 2016, pp. 615–629.
- [26] V. A. Sindagi and V. M. Patel, “Cnn-based cascaded multi-task learning of high-level prior and density estimation for crowd counting,” in *2017 14th IEEE international conference on advanced video and signal based surveillance (AVSS)*. IEEE, 2017, pp. 1–6.
- [27] Y. Zhang, D. Zhou, S. Chen, S. Gao, and Y. Ma, “Single-image crowd counting via multi-column convolutional neural network,” in *Proceedings of the IEEE conference on computer vision and pattern recognition*, 2016, pp. 589–597.
- [28] P. Sermanet, S. Chintala, and Y. LeCun, “Convolutional neural networks applied to house numbers digit classification,” in *Proceedings of the 21st international conference on pattern recognition (ICPR2012)*. IEEE, 2012, pp. 3288–3291.
- [29] S. Kumagai, K. Hotta, and T. Kurita, “Mixture of counting cnns: Adaptive integration of cnns specialized to specific appearance for crowd counting,” *arXiv preprint arXiv:1703.09393*, 2017.
- [30] A. Radford, J. W. Kim, C. Hallacy, A. Ramesh, G. Goh, S. Agarwal, G. Sastry, A. Askell, P. Mishkin, J. Clark *et al.*, “Learning transferable visual models from natural language supervision,” in *International conference on machine learning*. PmLR, 2021, pp. 8748–8763.
- [31] S. Liu, Z. Zeng, T. Ren, F. Li, H. Zhang, J. Yang, Q. Jiang, C. Li, J. Yang, H. Su *et al.*, “Grounding dino: Marrying dino with grounded pre-training for open-set object detection,” in *European Conference on Computer Vision*. Springer, 2024, pp. 38–55.
- [32] C. Liu, Y. Zhong, A. Zisserman, and W. Xie, “Countr: Transformer-based generalised visual counting,” *arXiv preprint arXiv:2208.13721*, 2022.
- [33] Z. You, K. Yang, W. Luo, X. Lu, L. Cui, and X. Le, “Few-shot object counting with similarity-aware feature enhancement,” in *Proceedings of the IEEE/CVF Winter Conference on Applications of Computer Vision*, 2023, pp. 6315–6324.
- [34] S. Kang, W. Moon, E. Kim, and J.-P. Heo, “Vlcounter: Text-aware visual representation for zero-shot object counting,” in *Proceedings of the AAAI Conference on Artificial Intelligence*, vol. 38, no. 3, 2024, pp. 2714–2722.
- [35] N. Dukić, A. Lukežič, V. Zavrtnik, and M. Kristan, “A low-shot object counting network with iterative prototype adaptation,” in *Proceedings of the IEEE/CVF International Conference on Computer Vision*, 2023, pp. 18 872–18 881.

- [36] S. Dai, J. Liu, and N.-M. Cheung, “Referring expression counting,” in *Proceedings of the IEEE/CVF Conference on Computer Vision and Pattern Recognition*, 2024, pp. 16 985–16 995.
- [37] N. Amini-Naieni, K. Amini-Naieni, T. Han, and A. Zisserman, “Open-world text-specified object counting,” *arXiv preprint arXiv:2306.01851*, 2023.
- [38] Z. Liu, Z. Sun, Y. Zang, X. Dong, Y. Cao, H. Duan, D. Lin, and J. Wang, “Visual-rft: Visual reinforcement fine-tuning,” *arXiv preprint arXiv:2503.01785*, 2025.
- [39] J. Pan, C. Liu, J. Wu, F. Liu, J. Zhu, H. B. Li, C. Chen, C. Ouyang, and D. Rueckert, “Medvlm-r1: Incentivizing medical reasoning capability of vision-language models (vlms) via reinforcement learning,” *arXiv preprint arXiv:2502.19634*, 2025.
- [40] Y. Zhan, Y. Zhu, S. Zheng, H. Zhao, F. Yang, M. Tang, and J. Wang, “Vision-r1: Evolving human-free alignment in large vision-language models via vision-guided reinforcement learning,” *arXiv preprint arXiv:2503.18013*, 2025.
- [41] J. Zhang, J. Huang, H. Yao, S. Liu, X. Zhang, S. Lu, and D. Tao, “R1-vl: Learning to reason with multimodal large language models via step-wise group relative policy optimization,” *arXiv preprint arXiv:2503.12937*, 2025.
- [42] J. Schulman, F. Wolski, P. Dhariwal, A. Radford, and O. Klimov, “Proximal policy optimization algorithms,” *arXiv preprint arXiv:1707.06347*, 2017.
- [43] Riis, “Aerial sheep dataset,” url <https://universe.roboflow.com/riis/aerial-sheep>, jun 2022, visited on 2023-01-02. [Online]. Available: <https://universe.roboflow.com/riis/aerial-sheep>
- [44] X. Zhong, G. Wang, W. Liu, Z. Wu, and Y. Deng, “Mask focal loss: a unifying framework for dense crowd counting with canonical object detection networks,” *Multimedia Tools and Applications*, pp. 1–23, 2024.
- [45] E. David, S. Madec, P. Sadeghi-Tehran, H. Aasen, B. Zheng, S. Liu, N. Kirchgeßner, G. Ishikawa, K. Nagasawa, M. A. Badhon *et al.*, “Global wheat head detection (gwhd) dataset: A large and diverse dataset of high-resolution rgb-labelled images to develop and benchmark wheat head detection methods,” *Plant Phenomics*, 2020.
- [46] R. Guerrero-Gómez-Olmedo, B. Torre-Jiménez, R. López-Sastre, S. Maldonado-Bascón, and D. O. noro Rubio, “Extremely overlapping vehicle counting,” in *Iberian Conference on Pattern Recognition and Image Analysis (IbPRIA)*, 2015.
- [47] Z. Wang, Y. Pang, C. Ulus, and X. Zhu, “Counting manatee aggregations using deep neural networks and anisotropic gaussian kernel,” *Scientific Reports*, vol. 13, no. 1, p. 19793, 2023.

VI. APPENDIX

A. Evaluation metrics

To comprehensively assess model performance, we employ additional evaluation metrics, including the coefficient of determination (R^2), Mean Absolute Percentage Error (MAPE), Pearson's correlation coefficient, and Spearman's rank correlation coefficient. Their definitions are provided below.

1) *Coefficient of Determination R^2* : The R^2 score measures how well the predicted values fit the actual values, indicating the proportion of variance explained by the model:

$$R^2 = 1 - \frac{\sum_{i=1}^n (y_i - \hat{y}_i)^2}{\sum_{i=1}^n (y_i - \bar{y})^2} \quad (10)$$

where y_i and \hat{y}_i denote the actual and predicted values, respectively, \bar{y} is the mean of the actual values, and n is the total number of samples. An R^2 value closer to 1 indicates a better fit.

2) *Mean Absolute Percentage Error (MAPE)*: MAPE quantifies the relative prediction error as a percentage, providing an intuitive measure of accuracy:

$$\text{MAPE} = \frac{1}{n} \sum_{i=1}^n \left| \frac{y_i - \hat{y}_i}{y_i} \right| \times 100 \quad (11)$$

A lower MAPE value indicates higher prediction accuracy. However, it is sensitive to small actual values, which can lead to inflated error percentages.

3) *Pearson's Correlation Coefficient*: Pearson's correlation coefficient (r) measures the linear relationship between predicted and actual values, ranging from -1 to 1:

$$r = \frac{\sum_{i=1}^n (y_i - \bar{y})(\hat{y}_i - \bar{\hat{y}})}{\sqrt{\sum_{i=1}^n (y_i - \bar{y})^2} \sqrt{\sum_{i=1}^n (\hat{y}_i - \bar{\hat{y}})^2}} \quad (12)$$

A value close to 1 indicates a strong positive correlation, while a value close to -1 suggests a strong negative correlation.

4) *Spearman's Rank Correlation Coefficient*: The Spearman's correlation (ρ) assesses the monotonic relationship between predicted and actual values by ranking the data points:

$$\rho = 1 - \frac{6 \sum d_i^2}{n(n^2 - 1)} \quad (13)$$

where d_i is the difference between the ranks of y_i and \hat{y}_i , and n is the number of observations. Unlike Pearson's correlation, Spearman's correlation captures non-linear relationships by evaluating rank similarity.